Engineered CpG-Antigen Conjugates Protected Gold Nanoclusters as Smart Self-Vaccines for Enhanced Immune Response and Cell Imaging

Yu Tao, Enguo Ju, Zhenhua Li, Jinsong Ren, and Xiaogang Qu**

A facile one-pot synthesis of fluorescent AuNCs by using ovalbumin-CpG oligodeoxynucleotides (ODNs) conjugates as the templates, which can elicit specific immunological responses, is demonstrated. Through dual-delivery of protein antigen and CpG ODNs, the as-prepared AuNCs can act as smart self-vaccines to assist in generation of high immunostimulatory activity while simultaneously act as an imaging agent. The AuNCs-based vaccines are not thought to have not been reported so far, making this platform the first example of the usage of AuNCs as effective vaccines. Furthermore, compared with the antigen, the immunostimulatory activity of the as-prepared AuNCs can not only be retained, but also can be effectively enhanced. These findings suggest the AuNCs-based vaccines may be utilized as safe and efficient immunostimulatory agents that are able to prevent and/or treat a variety of ailments.

1. Introduction

While conventional live vaccines provide an effective vaccination strategy devised since the beginning of the vaccinology era,[1] safety concerns may impede their clinical utility, necessitating the development of safer vaccines.[2] In this regard, modern vaccines, such as protein antigen-based subunit vaccines, are becoming increasingly viable alternatives for immunotherapy.[3] These synthetic subunit vaccines offer potential benefits over live or attenuated vaccine vectors in some disease applications, including improved safety, ease of manufacturability, reduced cost, and control over the antigen specificity of the immune response.[4] General shortcomings, however, including rapid degradation in vivo by blood proteases, inefficient uptake by professional antigen presenting cells (APCs), as well as the typically weak and short-lived humoral and cellular immune responses still seriously limit their further development as effective vaccines.[5] To improve the immunogenicity of subunit vaccines, immune adjuvants are often added to the formulation.[6] The discovery of Toll like receptor 9 (TLR9) ligands containing nonmethylated CpG motifs have provided a family of novel and relatively safe Th1-promoting adjuvants.[7] CpG oligodeoxynucleotides (CpG ODNs) are able to mimic molecular signatures of pathogens and trigger an immunostimulatory cascade including maturation, differentiation, and proliferation of multiple host immune cells through pattern recognition receptors, which can thus greatly enhance the potency of the vaccine.[8] While the usage of CpG has demonstrated an enhancement of immunity,[9] recent studies have shown that antigens and CpG ODNs must be co-localized in the same APCs to generate the most potent therapeutic antigen-specific immune responses.[10] Therefore, the close proximity of the protein antigen and CpG oligonucleotides adjuvant, especially, direct linkage of CpG ODNs to an antigen, ensuring that antigens and CpG ODNs can co-deliver to the same APCs, is critical to induce strong and long-term immunity.[7],[10d] New advances in materials sciences have created the possibility of delivering antigen and adjuvant on a single platform. To date, various carriers, including mesoporous silica nanoparticles,[6] gold nanoparticles,[11] nanoliposomes,[12] pH-responsive polymers,[13] polyelectrolyte multilayer capsules,[14] lanthanides-based core–shell nanoparticles,[7] PLGA microparticles,[15] DNA tetrahedron,[10d] and nanolipoprotein particles,[16] have been introduced for effective co-delivery of CpG ODNs and antigens into APCs. Although great progress has been achieved in this field, effective methods for facile synthesis of the simple yet efficient vaccine delivery vehicles are still much in demand.

On the other hand, noble metal nanoclusters, which consist of only several to tens of metal atoms and possess sizes comparable to the Fermi wavelength, have become a burgeoning area of scientific interest.[17] Among these metal clusters, the gold nanoclusters (AuNCs) have drawn particular attention owing to their unique features, including ease of generation, good water solubility, high biocompatibility, excellent stability, and strong fluorescence. These advantages have led to the use of AuNCs in biochemical and analytical chemistry research.[18] Recently, biological templates, especially proteins, for the generation of AuNCs are increasingly employed.[17a],[19] Compared with

Y. Tao, E. Ju, Z. Li, Prof. J. Ren, Prof. X. Qu
State Key laboratory of Rare Earth Resources Utilization and Laboratory of Chemical Biology
Changchun Institute of Applied Chemistry
Chinese Academy of Sciences
Changchun, 130022, China
E-mail: jren@ciac.jl.cn; xqu@ciac.jl.cn
Y. Tao, E. Ju, Z. Li
Graduate School of the Chinese Academy of Sciences
Beijing, 100039, China

DOI: 10.1002/adfm.201302347

organic molecules protected AuNCs, the usage of proteins as a green chemical reducing and stabilizing agent is advantageous because of their favorable biocompatibility, excellent aqueous dispersibility, and robust pH-stability.[17a],[19d] More recently, the protein-protected AuNCs have been reported to retain their bioactivity. For example, Chou and co-workers showed the synthesis of the insulin-templated fluorescent AuNCs, which maintained the insulin bioactivity.[19d] Additionally, lysozyme-protected AuNCs were demonstrated to exhibit excellent antimicrobial activity against the antibiotic-resistant bacteria by Chen and co-workers.[19g] Although significant effort has been devoted to preparing AuNCs for biological applications, to the best of our knowledge, the AuNCs-based vaccines have not been explored until now. To fulfill the requirements of an effective and simple vaccine, here we report the facile one-pot synthesis of fluorescent AuNCs by using ovalbumin (OVA) as a template, which can elicit specific immunological responses. OVA is often used as a model antigen due to its well established antigenic properties and capacity to induce strong cellular immunity via T lymphocytes as well as humoral immunity via B lymphocytes.[20] The resulting OVA-AuNCs (OAs) exhibit intense red fluorescence, and more importantly, compared with OVA, the immunostimulatory activity of the as-prepared OAs can not only be retained, but also can be effectively enhanced. This represents the first use of AuNCs to improve the antigen-specific immune responses. Moreover, the CpG ODNs can further be covalently linked to OVA (OVA-CpG ODNs conjugates), which can also be used as a template for the synthesis of AuNCs (OVA-AuNCs-CpG conjugates, OACs). The OACs are able to efficiently deliver the adjuvant CpG ODNs and the antigen OAs to the same antigen-presenting cells. Meanwhile, the capacity of preventing the degradation of the CpG ODNs and the antigen protein also endows the OACs with the ability to act as self-vaccines to assist in generation of enhanced immune response (**Scheme 1**). Here, we also provide the first evidence that the OACs can induce strong immune responses in vivo, highlighting the potential of OACs to serve as promising self-vaccines for immunotherapy. Significantly, the fascinating optical property also enables the OACs as a promising optical probe for fluorescent imaging.

2. Results and Discussion

Detailed synthetic procedures were elaborated in the Supporting Information. In brief, sulfydryl-tagged CpG ODNs were first covalently conjugated with OVA using 4-Maleimidobutyric acid N-hydroxysuccinimide ester (GMBS) as the cross-linking agent. PAGE was used for qualitative evaluation of the ratios of CpG ODNs:OVA. As can be seen in Figure S1 (Supporting Information), a ladder was visible corresponding to increasing CpG ODNs:OVA ratios in the OVA-CpG conjugates. The average molar ratio of CpG ODNs:OVA was ≈2:1. After that, the OACs were prepared according to the method proposed by Ying and co-workers.[17a] Without the covalent linkage of CpG ODNs, the same procedure gave the control (OAs). The optical absorption (Figure S2, Supporting Information) and fluorescence properties of the as-prepared OACs were firstly studied. As shown in **Figure 1**a, the OACs exhibited remarkably strong emission (ex = 490 nm/em = 595 nm), and were found to be stable for several months (data not shown). In addition, the zeta potentials of the OAs and OACs were also characterized (Figure S3, Supporting Information). The zeta potentials of OVA, OAs and the OACs were –35.4 mV, –25.4 mV, and –29.5 mV, respectively. As robust pH stability was essential to bioapplications,[21] we thus further interrogated the pH stability of AuNCs. Notably, no obvious photobleaching was observed over a broad pH range of 1–14, demonstrating the good fluorescence stability of AuNCs in different acidic/basic media (Figure S4, Supporting Information). Figure 1b displayed a high-resolution transmission electron microscopy (HRTEM) image of the OACs. The size of the AuNCs was estimated to be 1.13 nm, indicating that a nanocluster contained approximately 44 Au atoms.[19g] In addition, we also estimated the number of OVA molecules bound to a single OVA-Au nanocluster. ICP-MS was used to estimate the amount of OVA in an OVA-Au nanocluster. On the basis of the ICP-MS results (Figure S5, Supporting Information), we estimated that there were approximately 3 OVA molecules bound to a single OVA-Au nanocluster. AFM was also recorded to confirm that the average size of the as-prepared OACs was less than 1.5 nm, consistent with TEM results (Figure S6, Supporting Information). In the following, verification of Au composition was provided by the energy-dispersive X-ray (EDS) spectrum of the OACs (Figure 1c). In addition, XPS spectra (Figure 1d) clearly showed two peaks centered at binding energies of 83.5 and 87.3 eV, which correspond to the Au 4f7/2 peak and Au 4f5/2 peak, respectively, further indicating the formation of the AuNCs.[22] After that, the stability of the OACs against nuclease degradation was measured in biological media. In a typical experiment, we incubated the OACs with 50% fetal bovine serum (FBS).[9d],[19d] The result in Figure S7

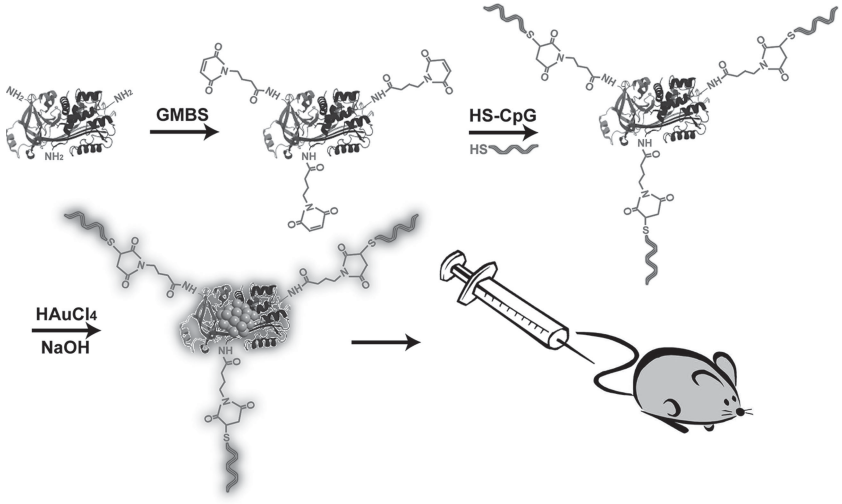

Scheme 1. General scheme for the synthesis of the OVA-AuNCs-CpG conjugates to induce immune response.

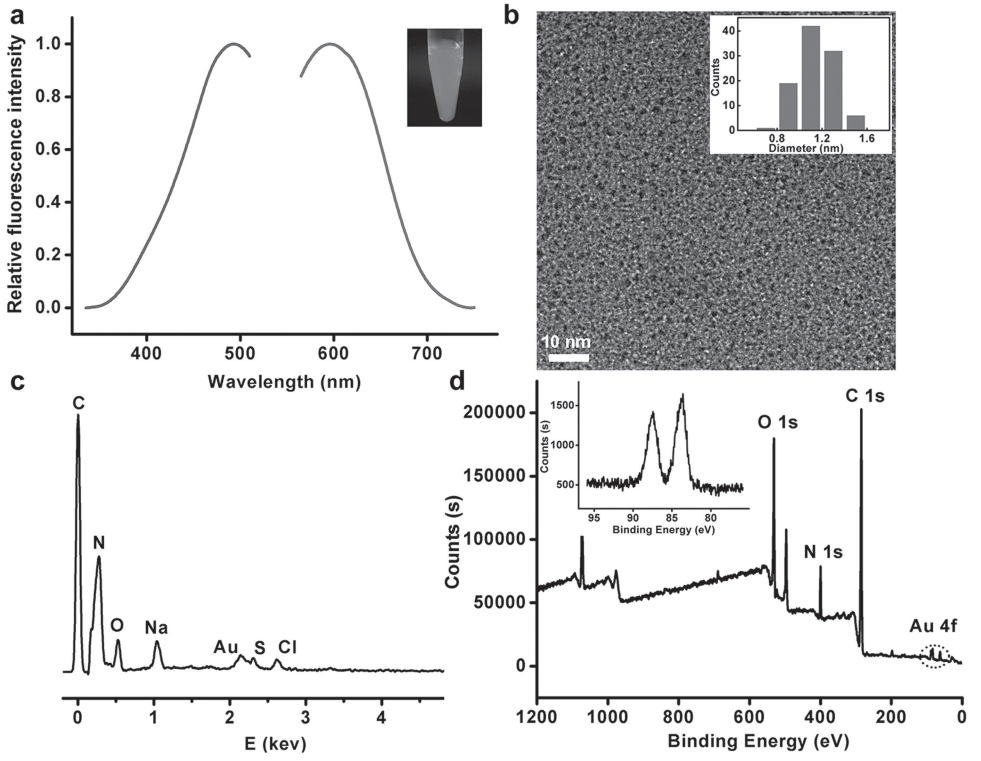

Figure 1. a) The excitation and emission fluorescence spectra of the as-prepared OVA-AuNCs-CpG conjugates. The insert photograph displays the luminescence of the AuNCs under a UV lamp. b) HRTEM image of the OVA-AuNCs-CpG conjugates. Scale bar: 10 nm. Insert: size distribution histogram of the OVA-AuNCs-CpG conjugates. The total number of clusters counted for the histogram was 100. c) EDS and d) XPS spectra of the as-synthesized OVA-AuNCs-CpG conjugates.

showed good stability, revealing that the AuNCs exhibited significant positive effects on the biological stability of the OACs.

Prior to the application of the OACs in cells or tissues, the potential cytotoxicity of the nanoplatform was first evaluated by a conventional methyl thiazolyl tetrazolium (MTT) assay (**Figure 2**a), which measured the mitochondrial activity of viable cells.[23] The viability of RAW264.7 cells was measured in the presence of the OAs and OACs at various concentrations (5–100 μg mL^{-1}). No apparent cellular toxicity of the OAs and OACs could be observed, even at the highest concentration (100 μg mL^{-1}). After that, the biocompatibilities of the OAs and OACs were also investigated by the lactate dehydrogenase (LDH) assay. Release of LDH was an indicator of cell membrane damage, which led to cell necrosis.[24] The results in Figure 2b similarly showed that cell viabilities of RAW264.7 exposed to the OAs and OACs were not affected. In addition, the cellular toxicity of OAs and OACs toward NIH 3T3 mouse embryonic fibroblast cells was also determined by means of a standard MTT cell assay (Figure S8, Supporting Information). It could be seen that OAs and OACs showed no significant cytotoxic effect on the NIH 3T3 cells in a wide range of concentration (5–100 μg mL^{-1}). All these assays demonstrated that the OAs and OACs exhibited extremely low cytotoxicity, revealing that they had high biocompatibility.

Motivated by the fascinating fluorescent properties and low cytotoxicity of the OACs, we then made attempts to explore the potential of the OACs for cell imaging, which provided an indication of the cellular uptake efficiency. Figure 2c–e showed the photoluminescence images of RAW264.7 cells after incubation with the FITC-labeled CpG ODNs, the OACs or the OACs with FITC-modified CpG ODNs. No fluorescence signal was detected in cells incubated with FITC-labeled CpG ODNs alone (Figure 2c), which was consistent with the facts that naked ODNs had difficulty passing the cytoplasmic membrane and were also prone to degradation by nucleases.[25] Remarkably, the cells gave out an extremely intense, red fluorescence after incubated with the OACs (Figure 2d), strongly suggesting that the AuNCs could act as a promising optical label for cell imaging. Overlays of the luminescence and bright-field images demonstrated that the luminescence was evident in the intracellular region, indicating that AuNCs could facilitate the intracellular delivery of the OACs. Furthermore, the co-localization of green/red fluorescence signals in Figure 2e supported the idea that both the antigens OAs and CpG ODNs were internalized in the same RAW264.7 cells, which would result in higher immunostimulatory activity as compared to the free OAs or CpG ODNs alone. All these results confirmed that the AuNCs could facilitate effective presentation of the antigen OVA and adjuvant CpG ODNs into the same TLR9-positive cells, which might significantly enhance immune activity.

The maturation of APCs was associated with the secretion of immunostimulatory cytokines such as TNF-α and IL-6.[26] As APCs activation was critical for immune responses, the effect of

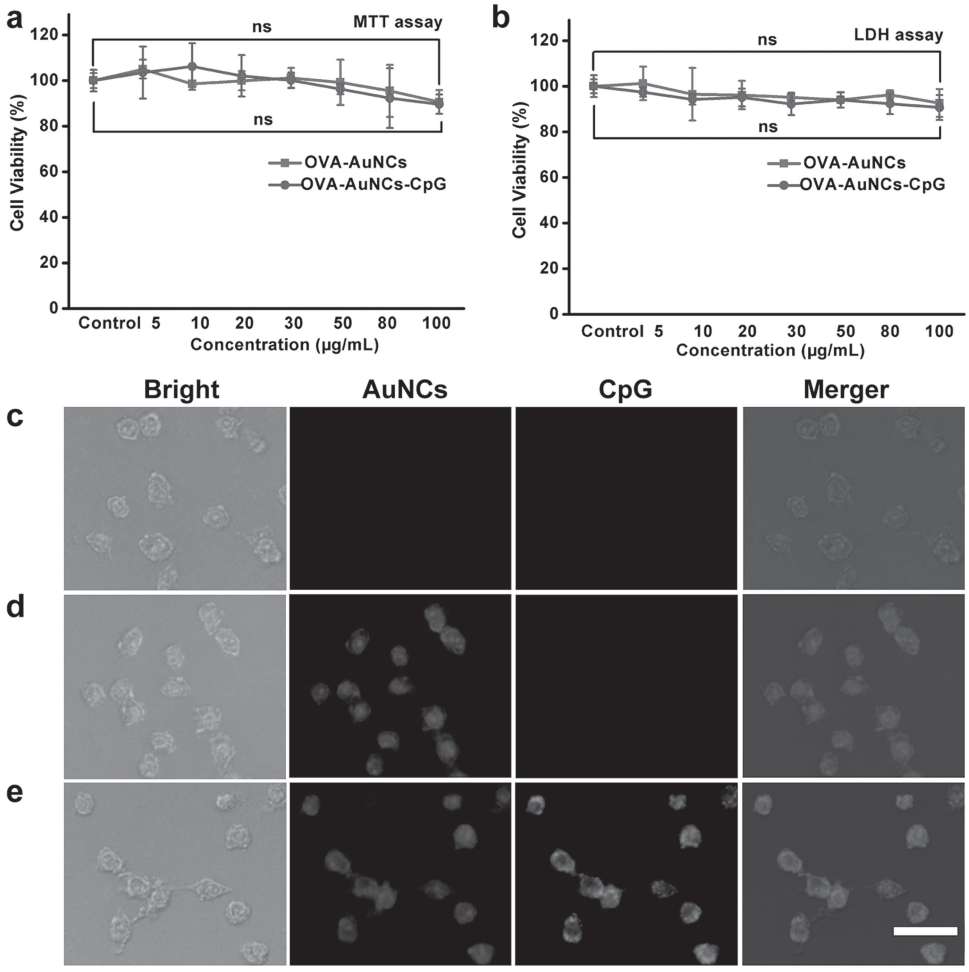

Figure 2. Cytotoxicity testing results of the OVA-AuNCs and the OVA-AuNCs-CpG conjugates against RAW264.7 cells by a) MTT and b) LDH assays. The concentration of the OVA was adopted to confirm the concentration of the OVA-AuNCs and the OVA-AuNCs-CpG conjugates in the following experiments. The values represent percentage cell viability (means ± SD, $n = 3$); ns = no significant difference ($P > 0.05$). Fluorescence images of RAW264.7 cells treated with c) FITC-labeled CpG ODNs (2 μM), d) the OVA-AuNCs-CpG conjugates (50 μg mL^{-1}) or e) the OVA-AuNCs-CpG conjugates with FITC-modified CpG ODNs (50 μg mL^{-1}). Scale bar: 20 μm.

nanovaccines on the activation of APCs was investigated by analyzing cytokine secretion levels. Samples were incubated with RAW264.7 cells and the levels of TNF-α and IL-6 secreted were recorded as a measure of immunostimulation. As can be seen in **Figure 3**a, the amount of the secreted TNF-α stimulated by OAs was more than 2-fold higher than that of free OVA. We used circular dichroism (CD) to investigate the effect of AuNCs on OVA secondary structure. As shown in Figure S9 (Supporting

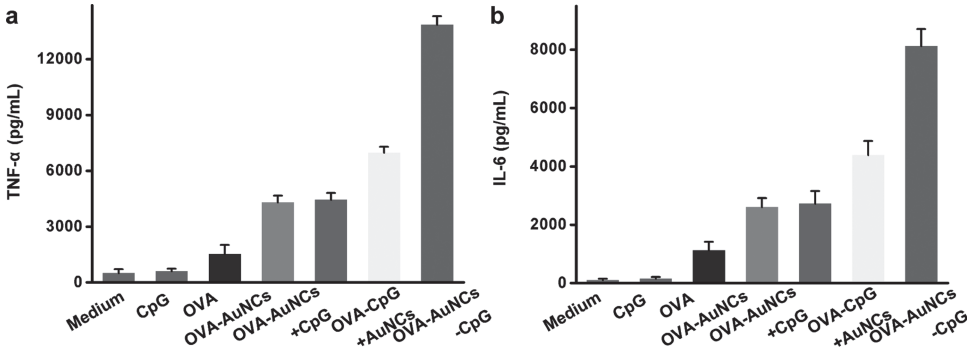

Figure 3. Cytokine release from RAW264.7 cells stimulated by the OVA-AuNCs-CpG conjugates. Comparison of a) TNF-α and b) IL-6 release stimulated by CpG ODNs (200 nM), OVA (5 μg mL^{-1}), OVA-AuNCs (5 μg mL^{-1}), OVA-AuNCs (5 μg mL^{-1}) + CpG ODNs (200 nM), OVA-CpG ODNs + AuNCs (5 μg mL^{-1}) and the OVA-AuNCs-CpG conjugates (5 μg mL^{-1}). Error bars represent standard deviation of three independent measurements.

Information), the encapsulation of AuNCs in OVA molecules had little effect on the structure of the OVA scaffolds, which provided the opportunity to preserve the bioactivity of the natural OVA. Besides, compared with OVA, the OAs offered additional benefits, such as higher cellular uptake efficiency and good stability, which thus can significantly increase the immunostimulatory efficacy. Notably, when comparing the OACs to a mere mixture of OAs and free CpG ODNs, the huge increase was noted on the level of TNF-α, clearly reflecting that concomitant delivery of antigens and CpG ODNs to the same APCs was indeed beneficial for the enhanced cellular immunity. Similarly, compared with the OVA and CpG control, the level of the other cytokine IL-6 (Figure 3b) induced by the OACs was also greatly increased. The high immunostimulatory activity of OACs could be attributed to the co-localized delivery of adjuvants and antigens to the same APCs. Other factors, such as enhanced cell uptake efficiency and increased stability of CpG ODNs and antigens, might also contribute to the increased immunostimulatory activity of OACs. Thus, these results demonstrated that, without the need of vaccine carriers, the OACs could act as self-vaccines to help in the generation of enhanced immunostimulatory activity.

As a result of the excellent immunostimulatory activity, we then moved one step further toward in vivo testing. To investigate the synergistic effects arising from the co-delivery of antigen and immunostimulatory agent to the same APCs in vivo, balb/c mice were vaccinated subcutaneously with samples described in the experimental section and the anti-OVA specific total serum IgG titres were measured. As shown in **Figure 4**a, mice receiving CpG ODNs only showed no specific antibody response and were similar to the unimmunized control mice group tested. In contrast, the amount of anti-OVA IgG vaccinated with OAs was about 2 fold more than that of the free OVA, demonstrating that, compared with OVA, the immunostimulatory activity of the OAs can be effectively enhanced. We reasoned the enhanced immunostimulatory effects were due to the fact that more OVA protein was protected from degradation before internalized by APCs. Notably, vaccination with the OACs resulted in much higher number of anti-OVA IgG compared to that of OAs mixed with free CpG ODNs. These data implied that covalent linkage of the TLR agonist, such as CpG, together with the antigen could serve as a promising strategy to induce potent antigen-specific cellular immunity. Next, to determine whether there were deleterious side effects associated with injection of the OACs, tissues from the organs were harvested from two mice for each group at the time of necropsy. Tissues including injection site, heart, liver, spleen, lung, and kidney were examined (Figure 4b).[20] Hemotoxylin and eosin staining of fixed tissues showed that there were no discernible morphological differences in the tissue at the site of injection in mice receiving the OACs compared to the unimmunized controls. Similarly, no morphological changes could be detected between all organs derived from animals in the unimmunized control group compared to the treatment groups receiving subcutaneous injections of OACs, which indicated that the self-vaccines OACs presented high biocompatibility and showed more promising for further immunotherapy.

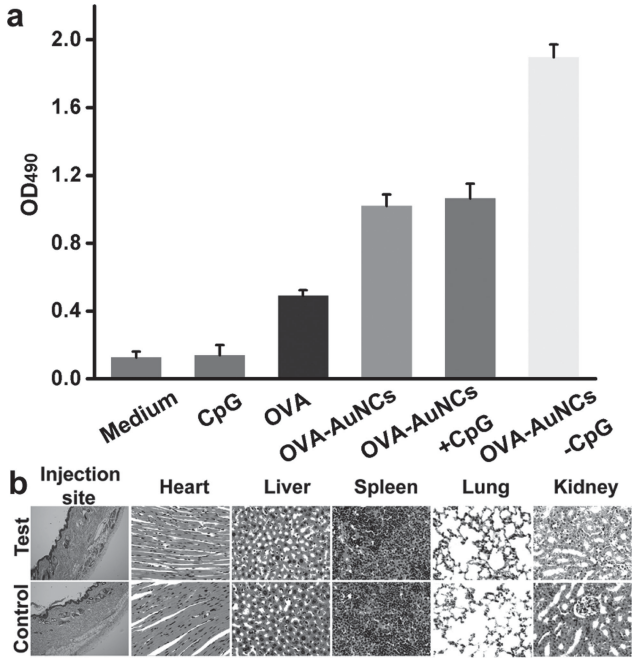

Figure 4. a) ELISA results of anti-OVA IgG titers elicited by different stimulus. b) Histopathological studies of tissue organs from a mouse injected with the OVA-AuNCs-CpG conjugates (top panel) and a non-immunized control animal (bottom panel). These organs are stained with haematoxylin and eosin (H&E) and observed under a light microscope. Tissues were harvested from injection site, heart, spleen, liver, lung, as well as kidney.

3. Conclusion

In summary, we have demonstrated, for the first time, that the antigen protein OVA can be covalently linked to the adjuvant CpG ODNs, which is able to be used as a template to produce highly fluorescent AuNCs. Through dual-delivery of protein antigen and CpG ODNs on AuNCs, the as-prepared OACs can act as smart self-vaccines to assist in generation of high immunostimulatory activity while simultaneously act as an imaging agent. To the best of our knowledge, the AuNCs-based vaccines have not been reported until now, making our platform the first example of the usage of AuNCs as effective vaccines. The introduction of the OACs brings about several unprecedented advantages. Firstly, the AuNCs are easy to synthesize, and have minimal cytotoxicity, which make them a kind of biocompatible nanomaterial for biomedical applications. Secondly, and more importantly, the OACs can simultaneously deliver antigens and CpG ODNs to the same APCs, thus can efficiently cause the activation of APCs along with effective antigen presentation. Both in vitro and in vivo experiments demonstrate that these engineered vaccines possess high immunogenicity. Finally, without the need of fluorophore labeling, the OACs with fascinating optical properties can also simultaneously serve as a promising optical probe for bioimaging. Collectively, taken together, these findings suggest the OACs may be utilized as safe and efficient immunostimulatory agents that are able to prevent and/or treat a variety of ailments.

4. Experimental Section

Materials and Instrumentation: Purified anti-mouse TNF-α, biotin conjugated anti-mouse TNF-α cocktail, TNF-α standard, anti-mouse IL-6, biotin anti-mouse IL-6 and IL-6 standard were purchased from eBioscience. OPD (o-phenylenediamine) substrate was purchased from DingGuo. Thiazolyl blue tetrazolium bromide (MTT) and ovalbumin (OVA) were purchased from Sigma-Aldrich (USA). Dulbecco's modified Eagle's medium (DMEM) and fetal Bovine Serum (FBS) were purchased from Invitrogen. The mouse leukemic monocyte macrophage cell line (RAW264.7 cell line) was purchased from Cell Bank of Chinese Academy of Sciences (Shanghai). $HAuCl_4$ and all other reagents were of analytical reagent grade, and used as received. Nanopure water (18.2 MΩ; Millpore Co., USA) was used in all experiments and to prepare all buffers. Sulfydryl-tagged CpG ODNs (5′-TCC ATG ACG TTC CTG ACG TT-SH-3′) were synthesized by Sangon Biotechnology Inc. (Shanghai, China).

Atomic-force microscopy (AFM) measurements were performed using Nanoscope V multimode atomic force microscope (Veeco Instruments, USA). Tapping mode was used to acquire the images under ambient conditions. Transmission electron microscopy (TEM) images were recorded using a FEI TECNAI G2 20 high-resolution transmission electron microscope operating at 200 kV. Fluorescence measurements were carried out on Jasco-FP-6500 spectra fluorometer (Jasco International Co. LTD. Tokyo, Japan). EDS was carried out using a HITACHI S-4500 instrument. Fluorescence images were captured using an Olympus BX-51 optical equiped with a CCD camera.

Synthesis of the OVA-CpG ODNs Conjugates: Ovalbumin was activated with a 20-fold molar excess of 4-maleimidobutyric acid n-hydroxysuccinimide ester (GMBS) at room temperature for 1 h. This modified the amino side chains of L-lysine residues by the addition of maleimide groups. Residual reagents were removed by chromatography on a G-25 desalting column. Then the sulfydryl-tagged CpG ODNs were reduced with 200 mM Tris-(2-carboxyethyl) phosphine (TCEP; Pierce) at room temperature for 1 h, and residual reagents were removed by chromatography on a G-25 desalting column. The resulting sulfydryl-tagged CpG ODNs were mixed with the modified OVA at a 5:1 molar ratio (CpG ODNs : OVA) and incubated overnight at room temperature. The concentration of the OVA was adopted to confirm the concentration of the OVA-CpG ODNs conjugates in the following experiments.

Synthesis of the OVA-AuNCs-CpG Conjugates: $HAuCl_4$ (10 mM, 1 mL) was vigorously stirred with the OVA-CpG ODNs conjugates (50 mg mL^{-1}, 1 mL) for 5 min initially, followed by the addition of NaOH (1 M, 100 μL) to adjust the pH of the solution to approximately pH 12. The mixture was then continually reacted under vigorous stirring at 37 °C for 24 h. The concentration of the OVA was adopted to confirm the concentration of the OVA-AuNCs-CpG conjugates in the following experiments.

Synthesis of the OVA-AuNCs: $HAuCl_4$ (10 mM, 1 mL) was vigorously stirred with the OVA (50 mg mL^{-1}, 1 mL) for 5 min initially, followed by the addition of NaOH (1 M, 100 μL) to adjust the pH of the solution to approximately pH 12. The mixture was then continually reacted under vigorous stirring at 37 °C for 24 h. The concentration of the OVA was adopted to confirm the concentration of the OVA-AuNCs in the following experiments.

Cell Culture: The murine macrophage-like RAW264.7 cells were grown at 37 °C in an atmosphere of 5 v/v% CO_2 in air, in Dulbecco's modified Eagle's medium (DMEM) supplemented with 10% heat-inactivated FBS, 1.5 g L^{-1} $NaHCO_3$, 100 units mL^{-1} penicillin, 100 mg mL^{-1} streptomycin, 4.5 g L^{-1} glucose and 4 mM glutamine. The media was changed every three days, and the cells were digested by trypsin and resuspended in fresh complete medium before plating.

Cytotoxicity Assays: MTT assays were used to probe cellular viability. RAW264.7 cells were seeded at a density of 5000 cells $well^{-1}$ (100 μL total volume $well^{-1}$) in 96-well assay plates. After 24 h incubation, the as-prepared OVA-AuNCs and OVA-AuNCs-CpG conjugates, at the indicated concentrations, were added for further incubation of 48 h. To determine toxicity, 10 μL of MTT solution (BBI) was added to each well of the microtiter plate and the plate was incubated in the CO_2 incubator for an additional 4 h. Then the cells were lysed by the addition of 100 μL of DMSO. Absorbance values of formazan were determined with Bio-Rad model-680 microplate reader at 490 nm (corrected for background absorbance at 630 nm). Three replicates were done for each treatment group.

LDH Assay: The cell membrane integrity can be determined by lactate dehydrogenase (LDH) leakage assay. RAW264.7 cells were seeded at a density of 20 000 cells/well in 96-well plates and allowed to settle overnight. Next, cells were incubated with the OVA-AuNCs and OVA-AuNCs-CpG conjugates at 0, 5, 10, 20, 30, 50, 80, and 100 μg mL^{-1}. After 48 h, an LDH assay was performed according to the manufacturer's protocol (Beyotime institute of biotechnology, China). Untreated cells were assayed as a negative control.

Fluorescent Microscopic Imaging: For the cell imaging test, the concentration of RAW264.7 cells was fixed at a density of 10^5 cells $well^{-1}$ in 24-well assay plates. Then the FITC-labeled CpG ODNs, the OVA-AuNCs-CpG conjugates and the OVA-AuNCs-CpG conjugates with FITC-modified CpG ODNs were separately added to the cells and incubated at 37 °C for 6 h. The cells were then washed several times with PBS. Finally the imagings were captured using an Olympus BX-51 optical equipped with a CCD camera.

Cytokine Assays: RAW264.7 cells were seeded on 6-well culture plates at a density of 5×10^5 cells/well. After 24 h incubation, cells were washed with 0.5 ml PBS before treatment with indicated conditions for 8 h (TNF-α) or 24 h (IL-6). The supernatants were collected and stored at –80 °C until use. The levels of TNF-α, and IL-6 in the supernatants were determined by enzymelinked immunosorbent assay (ELISA) using antibody pairs specific to these cytokines following protocols recommended by the manufacturer.

Immunogenicity Study: Balb/C mice of 4–6 weeks were purchased from Medical Experimental Animal Center of Jilin University (Changchun, China). Female Balb/C mice were divided into different groups with four mice in each group. Mice were immunized with various equivalent dose samples through subcutaneous injection. The amount of the OVA-AuNCs-CpG conjugates is 200 μg mL^{-1} (100 μL) at each time point. The dose of OVA, OVA-AuNCs, and OVA-AuNCs + CpG ODNs was the same as that of the OVA-AuNCs-CpG conjugates and the amount of CpG ODNs is 8 μM (100 μL) at each time point. The concentration of OVA was adopted to confirm the concentration of OVA-AuNCs, OVA-AuNCs + CpG ODNs, and the OVA-AuNCs-CpG conjugates. Mice were injected on days 0, 14, and 28, and sera were collected on day 42. All animal procedures were in accord with the guidelines of the Institutional Animal Care and Use Committee.

Titer Measurements: Micro titer plates (Nunc, Roskilde, Denmark) were coated with OVA by incubation of 100 μL 20 μg mL^{-1} OVA in coating buffer (PBS, pH 7.2) for 24 h at 4 °C. To reduce aspecific binding, wells were blocked with 200 μL 1 w/v% BSA in PBST (0.05% Tween-20) for 1 h at 37 °C. After extensive washing with PBST, 20 dilutions of serum were added. After incubation for 1.5 h at 37 °C and washed three times, the second antibody of Anti-Mouse IgG (whole molecule)-Peroxidase antibody produced in goat was diluted to 1/2000 and incubated (100 μL per well) for 1 h at 37 °C. After washed four times, 0.4 mg mL^{-1} o-phenylenediamine (4 mg o-phenylenediamine was dissolved in a buffer containing 4.86 mL 0.1 M critic acid and 5.14 mL 0.2 M Na_2HPO_4) with 30% H_2O_2 (0.5 μL mL^{-1}) was added to wells (100 μL per well) as substrate. After 30 min incubation at room temperature, the color development was stopped by adding 50 μL of Stop Solution (2 M H_2SO_4) and optical absorption was measured at 490 nm.

Statistical Analysis: All data were expressed in this article as mean result ± standard deviation (SD). All figures shown in this article were obtained from three independent experiments with similar results. The statistical analysis was performed by using Origin 8.0 software.

Supporting Information

Supporting Information is available from the Wiley Online Library or from the author.

Acknowledgements

Financial support was provided by the National Basic Research Program of China (2011CB936004 and 2012CB720602) and the National Natural Science Foundation of China (21072182, 91213302, 21210002).

Received: July 12, 2013
Revised: August 15, 2013
Published online: September 20, 2013

[1] a) F. Fenner, D. A. Henderson, I. Arita, Z. Jezek, I. D. Landyi, *Smallpox and its eradication*, World Health Organization, Geneva **1988**; b) R. Rappuoli, H. I. Miller, S. Falkow, *Science* **2002**, *297*, 937; c) R. Rappuoli, C. W. Mandl, S. Black, E. De Gregorio, *Nat. Rev. Immunol.* **2011**, *11*, 865; d) G. Wang, R.-Y. Cao, R. Chen, L. Mo, J.-F. Han, X. Wang, X. Xu, T. Jiang, Y.-Q. Deng, K. Lyu, S.-Y. Zhu, E.-D. Qin, R. Tang, C.-F. Qin, *Proc. Natl. Acad. Sci. U. S. A.* **2013**, *110*, 7619.

[2] W. Byrd, A. de Lorimier, Z. R. Zheng, F. J. Cassels, *Adv. Drug Delivery Rev.* **2005**, *57*, 1362.

[3] B. Guy, *Nat. Rev. Microbiol.* **2007**, *5*, 505.

[4] a) M. Black, A. Trent, M. Tirrell, C. Olive, *Expert Rev. Vaccines* **2010**, *9*, 157; b) Y. Perrie, A. R. Mohammed, D. J. Kirby, S. E. McNeil, V. W. Bramwell, *Int. J. Pharm.* **2008**, *364*, 272.

[5] a) J. J. Moon, B. Huang, D. J. Irvine, *Adv. Mater.* **2012**, *24*, 3724; b) J. A. Hubbell, S. N. Thomas, M. A. Swartz, *Nature* **2009**, *462*, 449; c) M.-L. De Temmerman, J. Rejman, J. Demeester, D. J. Irvine, B. Gander, S. C. De Smedt, *Drug Discov. Today* **2011**, *16*, 569; d) A. Sexton, P. G. Whitney, S.-F. Chong, A. N. Zelikin, A. P. R. Johnston, R. De Rose, A. G. Brooks, F. Caruso, S. J. Kent, *Acs Nano* **2009**, *3*, 3391.

[6] N. Mitter, C. Yu, K. T. Mody, A. Popat, D. Mahony, A. S. Cavallaro, *Nanoscale* **2013**, *5*, 5167.

[7] Z. Li, Z. Liu, M. Yin, X. Yang, J. Ren, X. Qu, *Adv. Healthcare Mater.* **2013**, DOI: 10.1002/adhm.201200364.

[8] a) H. Liu, B. Kwong, D. J. Irvine, *Angew. Chem. Int. Ed.* **2011**, *50*, 7052; b) G. J. Weiner, H.-M. Liu, J. E. Wooldridge, C. E. Dahle, A. M. Krieg, *Proc. Natl. Acad. Sci. U. S. A.* **1997**, *94*, 10833.

[9] a) M. Wei, N. Chen, J. Li, M. Yin, L. Liang, Y. He, H. Song, C. Fan, Q. Huang, *Angew. Chem. Int. Ed.* **2012**, *51*, 1202; b) K. Mohri, M. Nishikawa, N. Takahashi, T. Shiomi, N. Matsuoka, K. Ogawa, M. Endo, K. Hidaka, H. Sugiyama, Y. Takahashi, Y. Takakura, *ACS Nano* **2012**, *6*, 5931; c) V. J. Schüller, S. Heidegger, N. Sandholzer, P. C. Nickels, N. A. Suhartha, S. Endres, C. Bourquin, T. Liedl, *ACS Nano* **2011**, *5*, 9696; d) J. Li, H. Pei, B. Zhu, L. Liang, M. Wei, Y. He, N. Chen, D. Li, Q. Huang, C. Fan, *ACS Nano* **2011**, *5*, 8783; e) G. Mutwiri, S. van Drunen Littel-van den Hurk, L. A. Babiuk, *Adv. Drug Delivery Rev.* **2009**, *61*, 226; f) M. Nishikawa, Y. Mizuno, K. Mohri, N. Matsuoka, S. Rattanakiat, Y. Takahashi, H. Funabashi, D. Luo, Y. Takakura, *Biomaterials* **2011**, *32*, 488.

[10] a) Y. Krishnamachari, A. K. Salem, *Adv. Drug Delivery Rev.* **2009**, *61*, 205; b) M. Diwan, M. Tafaghodi, J. Samuel, *J. Controlled Release* **2002**, *85*, 247; c) V. Sokolova, T. Knuschke, A. Kovtun, J. Buer, M. Epple, A. M. Westendorf, *Biomaterials* **2010**, *31*, 5627; d) X. Liu, Y. Xu, T. Yu, C. Clifford, Y. Liu, H. Yan, Y. Chang, *Nano Lett.* **2012**, *12*, 4254; e) A. D. Sandler, H. Chihara, G. Kobayashi, X. Zhu, M. A. Miller, D. L. Scott, A. M. Krieg, *Cancer Res.* **2003**, *63*, 394; f) H. J. Cho, K. Takabayashi, P. M. Cheng, M. D. Nguyen, M. Corr, S. Tuck, E. Raz, *Nat. Biotechnol.* **2000**, *18*, 509.

[11] I.-H. Lee, H.-K. Kwon, S. An, D. Kim, S. Kim, M. K. Yu, J.-H. Lee, T.-S. Lee, S.-H. Im, S. Jon, *Angew. Chem. Int. Ed.* **2012**, *51*, 8800.

[12] a) C. D. Andrews, M.-S. Huh, K. Patton, D. Higgins, G. Van Nest, G. Ott, K.-D. Lee, *Mol. Pharm.* **2012**, *9*, 1118; b) W. M. Li, W. H. Dragowska, M. B. Bally, M.-P. Schutze-Redelmeier, *Vaccine* **2003**, *21*, 3319.

[13] a) T. T. Beaudette, E. M. Bachelder, J. A. Cohen, A. C. Obermeyer, K. E. Broaders, J. M. J. Fréchet, E.-S. Kang, I. Mende, W. W. Tseng, M. G. Davidson, E. G. Engleman, *Mol. Pharm.* **2009**, *6*, 1160; b) J. T. Wilson, S. Keller, M. J. Manganiello, C. Cheng, C.-C. Lee, C. Opara, A. Convertine, P. S. Stayton, *ACS Nano* **2013**, *7*, 3912.

[14] B. G. De Geest, M. A. Willart, B. N. Lambrecht, C. Pollard, C. Vervaet, J. P. Remon, J. Grooten, S. De Koker, *Angew. Chem. Int. Ed.* **2012**, *51*, 3862.

[15] B. S. Román, J. M. Irache, S. Gómez, N. Tsapis, C. Gamazo, M. S. Espuelas, *Eur. J. Pharm. Biopharm.* **2008**, *70*, 98.

[16] N. O. Fischer, A. Rasley, M. Corzett, M. H. Hwang, P. D. Hoeprich, C. D. Blanchette, *J. Am. Chem. Soc.* **2013**, *135*, 2044.

[17] a) J. P. Xie, Y. G. Zheng, J. Y. Ying, *J. Am. Chem. Soc.* **2009**, *131*, 888; b) Z. Shen, H. W. Duan, H. Frey, *Adv. Mater.* **2007**, *19*, 349; c) H. Kawasaki, K. Hamaguchi, I. Osaka, R. Arakawa, *Adv. Funct. Mater.* **2011**, *21*, 3508; d) J. H. Yu, S. Choi, R. M. Dickson, *Angew. Chem. Int. Ed.* **2009**, *48*, 318.

[18] a) M. Zheng, X. Y. Huang, *J. Am. Chem. Soc.* **2004**, *126*, 12047; b) C.-C. Huang, C.-T. Chen, Y.-C. Shiang, Z.-H. Lin, H.-T. Chang, *Anal. Chem.* **2009**, *81*, 875; c) C. Wang, J. Li, C. Amatore, Y. Chen, H. Jiang, X.-M. Wang, *Angew. Chem. Int. Ed.* **2011**, *50*, 11644; d) J. Liu, M. Yu, C. Zhou, S. Yang, X. Ning, J. Zheng, *J. Am. Chem. Soc.* **2013**, *135*, 4978.

[19] a) H. Wei, Z. D. Wang, L. M. Yang, S. L. Tian, C. J. Hou, Y. Lu, *Analyst* **2010**, *135*, 1406; b) Y. H. Lin, W. L. Tseng, *Anal. Chem.* **2010**, *82*, 9194; c) F. Wen, Y. Dong, L. Feng, S. Wang, S. Zhang, X. Zhang, *Anal. Chem.* **2011**, *83*, 1193; d) C.-L. Liu, H.-T. Wu, Y.-H. Hsiao, C.-W. Lai, C.-W. Shih, Y.-K. Peng, K.-C. Tang, H.-W. Chang, Y.-C. Chien, J.-K. Hsiao, J.-T. Cheng, P.-T. Chou, *Angew. Chem. Int. Ed.* **2011**, *50*, 7056; e) L. Yan, Y. Cai, B. Zheng, H. Yuan, Y. Guo, D. Xiao, M. M. F. Choi, *J. Mater. Chem.* **2012**, *22*, 1000; f) Y. Yue, T.-Y. Liu, H.-W. Li, Z. Liu, Y. Wu, *Nanoscale* **2012**, *4*, 2251; g) W. Y. Chen, J. Y. Lin, W. J. Chen, L. Y. Luo, E. W. G. Diau, Y. C. Chen, *Nanomedicine* **2010**, *5*, 755.

[20] D. Mahony, A. S. Cavallaro, F. Stahr, T. J. Mahony, S. Z. Qiao, N. Mitter, *Small* **2013**, DOI: 10.1002/smll.201300012.

[21] Y. Zhong, F. Peng, F. Bao, S. Wang, X. Ji, L. Yang, Y. Su, S.-T. Lee, Y. He, *J. Am. Chem. Soc.* **2013**, *135*, 8350.

[22] W. Zhao, F. Gonzaga, Y. Li, M. A. Brook, *Adv. Mater.* **2007**, *19*, 1766.

[23] J. Moskovitz, P. Maiti, D. H. J. Lopes, D. B. Oien, A. Attar, T. Liu, S. Mittal, J. Hayes, G. Bitan, *Biochemistry* **2011**, *50*, 10687.

[24] L. Cheng, C. Wang, X. Ma, Q. Wang, Y. Cheng, H. Wang, Y. Li, Z. Liu, *Adv. Funct. Mater.* **2012**, *23*, 272.

[25] J. Mao, X. Cao, J. Zhen, H. Shao, H. Gu, J. Lu, J. Y. Ying, *J. Mater. Chem.* **2011**, *21*, 11478.

[26] A. Langenkamp, M. Messi, A. Lanzavecchia, F. Sallusto, *Nat. Immunol.* **2000**, *1*, 311.